Bull. Mater. Sci. (2019) 42:83
https://doi.org/10.1007/s12034-019-1741-4

Unique identification of phonon modes using polarized Raman studies of SnO(001) crystals

RAKTIMA BASU[1], D SORNADURAI[2], S AMIRTHAPANDIAN[3] and SANDIP DHARA[1,*]

[1]Surface and Nanoscience Division, Indira Gandhi Centre for Atomic Research, Homi Bhabha National Institute, Kalpakkam 603102, India
[2]Condensed Matter Physics Division, Indira Gandhi Centre for Atomic Research, Kalpakkam 603102, India
[3]Materials Physics Division, Indira Gandhi Centre for Atomic Research, Homi Bhabha National Institute, Kalpakkam 603102, India
*Author for correspondence (dhara@igcar.gov.in)

MS received 9 June 2018; accepted 9 August 2018; published online 15 March 2019

Abstract. Stannous oxide (SnO), an exclusive p-type oxide semiconductor in the oxide family, is a source of renewed interest because of its ability to be an excellent anode material. So far, there are very few reports on the vibrational properties of SnO and controversy remains in the assignment of vibrational modes. Textured single crystals of SnO were synthesized by a one-step solvothermal method. The as-synthesized SnO crystals have a wide (001) plane, as confirmed by high resolution transmission electron microscopy images. Raman spectroscopy is used for the identification of phase as well as crystalline orientation. Moreover, a unique assignment of phonon modes in SnO is also performed using polarized Raman spectroscopic studies for different orientations around *c*-axis of the crystal with the incident electric field vector. Thus, a novel methodology of phonon assignment is adopted with a minimum amount of data collection for a diatomic molecule having a tetragonal symmetry with a number of symmetry elements.

Keywords. Polarized Raman spectroscopy; SnO; Raman mode; solvothermal technique; crystal orientation.

1. Introduction

Stannous oxide (SnO) finds significant applications in thin film transistors [1], coating substances, as a catalyst for the polymerization of lactic acids [2–4] and as a precursor for the production of SnO_2, which is an important electronic grade material for sensor applications [5]. SnO is a p-type semiconductor with a direct optical band gap in the range of 2.7–3.4 eV and is recently found to be a promising anode material for lithium-ion rechargeable batteries [6,7]. It is well known that the optical properties of the material are determined by its structural symmetry. As the properties of metal oxides depend on unique structures and morphologies, various SnO structures such as particles, meshes, sheets, belts and blocks are being synthesized by a variety of methods [6,8–11]. There are very few reports on the vibrational properties of SnO [12,13]. Two Raman peaks at 114 and 211 cm^{-1} are reported for SnO [14,15]. However, controversy remains in the assignment of the peaks both in theoretical calculations and experimental reports [15–19]. Although the Raman peak at 210 cm^{-1} is identified as A_{1g} mode, there is a conflict in the assignment of the peak centred at 110 cm^{-1}. The peak is assigned as E_g mode as well as B_{1g} mode in the experimental reports of a polycrystalline sample [15,16]. However, for a randomly oriented polycrystalline structure, the assignment of Raman modes may be obscure at times, as the net intensity may lead to zero or get reduced for two oppositely oriented crystallites. On the other hand, low-frequency E_g mode ranges from 113 to 143 cm^{-1}, while B_{1g} mode is speculated between 350 and 370 cm^{-1} according to theoretical calculations [18,19]. Thus, a systematic polarized Raman study on oriented SnO single crystal is required for the definite assignment of the mode frequencies.

In the present study, we have reported detailed structural and vibrational properties of SnO(001) single crystals. Raman spectroscopy is used as an easy tool for the identification of phase as well as crystalline orientation. Polarized Raman spectroscopic analysis is used for the identification of different phonon modes in tetragonal SnO.

2. Experimental

SnO crystals were synthesized in a hydrothermal process using $SnCl_2$ (10 mM) dissolved in equal volume of dimethyl formamide and water solvent (40 ml of each) in a Teflon lined stainless steel autoclave. The reaction was carried out at 140°C for 72 h. The auto-cooled solution was filtered and washed with distilled water and dried at 60°C for 30 min yielding bluish black coloured iridescent cubic- and cuboidal-shaped crystals. Compositional stability and detailed synthesis process are reported elsewhere [20].

Morphological analysis of the pristine sample was studied using a field emission scanning electron microscope (FESEM, SUPRA 55 Zeiss). The structural and crystallographic nature of the SnO crystals was investigated using high resolution transmission electron microscopy (HRTEM, LIBRA 200FE Zeiss). The TEM sample was prepared by dispersing in a Cu grid by using isopropyl alcohol. The vibrational modes of the pristine sample were studied by Raman spectroscopic analysis using a micro-Raman spectrometer (inVia, Renishaw, UK) in the backscattering configuration with an Ar^+ laser (514.5 nm) as the excitation source, diffraction gratings of 1800 g mm^{-1} as a monochromator and a thermoelectrically cooled CCD camera as the detector. The spectra were collected using 50× objective with a numerical aperture of 0.35. To perform polarized Raman studies, half-wave plates and polarizer were inserted accordingly in the scattered ray path to achieve the required configurations.

3. Results and discussion

The tetragonal structure of SnO belongs to the $P4/nmm$ (D_{4h}) space group. The schematic structure (figure 1a) is layered with an AAK stacking sequence of slabs consisting of O ions sandwiched between Sn ions. The Sn ions form four square pyramidal bonds with Os [13]. The Cartesian X, Y and Z axes are chosen along a, b and c directions of the crystal, respectively (figure 1a). Detailed structural studies are reported earlier [20].

FESEM image (figure 1b) of the grown sample shows a typical single microcrystal of dimension ~300 × 100 μm. The inset of figure 1b shows the corresponding optical image of the microcrystal. HRTEM images were acquired for the pristine SnO crystals to identify the crystallographic orientation of the samples used for optical measurements. Figure 2 shows HRTEM lattice images and the corresponding fast Fourier transform (FFT) pattern of the SnO crystal.

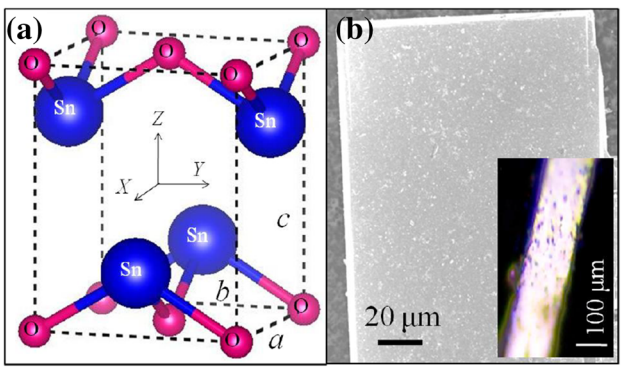

Figure 1. (**a**) Schematic structural diagram of SnO unit cell. The Cartesian X, Y and Z axes are chosen along a, b and c directions of the crystal, respectively. (**b**) FESEM image of the as-grown microcrystal. The inset shows corresponding optical image of the crystal.

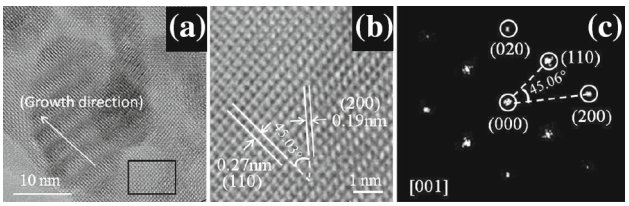

Figure 2. (**a**) HRTEM images of the as-synthesized SnO crystal. Arrow indicates the growth direction. (**b**) Enlarged image of the selected area from (**a**) showing (*hkl*) planes and (**c**) the corresponding FFT pattern of tetragonal phase of SnO with zone axes [001].

In the HRTEM image (figure 2a) and the magnified TEM image (figure 2b), the inter-planar spacing (d) values are found to be 0.27 and 0.19 nm, which match with the reported d values for the (110) and (200) planes of SnO, respectively (JCPDS card no. 06-0395). The corresponding FFT pattern of the SnO crystal (figure 2c) is indexed to the tetragonal phase of single-crystal SnO with zone axes along [001]. In both HRTEM image and FFT pattern, the angle between the planes is 45°. The TEM analysis confirms that the growth direction of the pristine SnO crystal (long axis) is along [110] and the crystal has a single-crystal-like structure with a wide, well-ordered (001) plane [21,22].

Raman spectroscopy is used to understand the vibrational properties of a material while interacting with electromagnetic excitation. The electric field vectors of the Raman scattered wave is associated with the electric field vector of the incident wave with a characteristic Raman tensor. There exists a unique Raman tensor for each Raman-active vibrational mode. The electric field vectors of the incident radiation ($\boldsymbol{E}_{xi}$; $\boldsymbol{E}_{yi}$; $\boldsymbol{E}_{zi}$) relates with the electric field vectors of the Raman scattered radiation ($\boldsymbol{E}_{xs}$; $\boldsymbol{E}_{ys}$; $\boldsymbol{E}_{zs}$) by the Raman tensor (R) as shown below:

$$\begin{pmatrix} E_{xs} \\ E_{ys} \\ E_{zs} \end{pmatrix} = \begin{pmatrix} R_{xx} & R_{xy} & R_{xz} \\ R_{yx} & R_{yy} & R_{yz} \\ R_{zx} & R_{zy} & R_{zz} \end{pmatrix} \begin{pmatrix} E_{xi} \\ E_{yi} \\ E_{zi} \end{pmatrix}. \quad (1)$$

Group theoretical analysis predicts four Raman active modes for SnO at Γ point, $A_{1g} + B_{1g} + 2E_g$. The corresponding Raman tensors are shown below [12,23]:

$$A_{1g}: \begin{pmatrix} a & 0 & 0 \\ 0 & a & 0 \\ 0 & 0 & b \end{pmatrix}; \quad B_{1g}: \begin{pmatrix} c & 0 & 0 \\ 0 & -c & 0 \\ 0 & 0 & 0 \end{pmatrix};$$

$$E_g: \begin{pmatrix} 0 & 0 & 0 \\ 0 & 0 & e \\ 0 & e & 0 \end{pmatrix}; \quad E_g: \begin{pmatrix} 0 & 0 & -e \\ 0 & 0 & 0 \\ -e & 0 & 0 \end{pmatrix}.$$

For textured single crystal of SnO(001), the incident and scattered electric field vectors can have components only

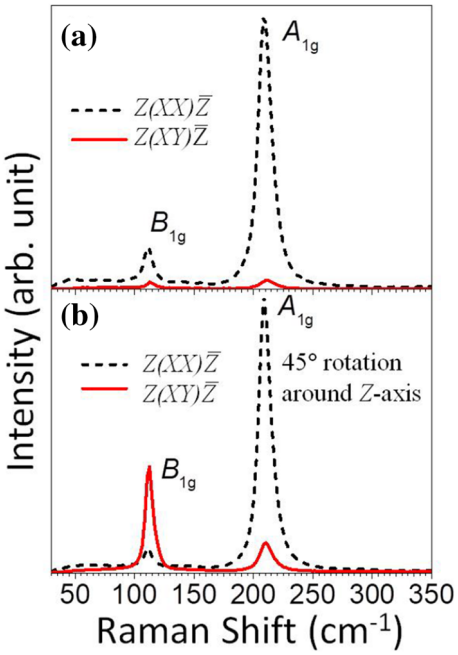

Figure 3. Raman spectra of the (001) textured SnO crystal at (**a**) $Z(XX)\bar{Z}$, $Z(XY)\bar{Z}$ polarization condition and (**b**) with a rotation of 45° around Z-axis in $Z(XX)\bar{Z}$, $Z(XY)\bar{Z}$ polarization condition.

along a and b crystal axes, as incident and scattered wave vectors are along Z and $\bar{Z}$ axes, respectively. From the above mentioned Raman tensors, it is clear that only A_{1g} and B_{1g} modes are allowed for the (001) textured crystals, as they have non-vanishing xx and yy tensor components. Using equation (1), one can find out both A_{1g} and B_{1g} modes, which are allowed in the $Z(XX)\bar{Z}$ and $Z(YY)\bar{Z}$ configurations. Whereas, no mode is allowed in the $Z(XY)\bar{Z}$ and $Z(YX)\bar{Z}$ configurations. The first and last letters in the Porto notation denote the incident and scattered wave vectors, respectively, and the letters within the parentheses denote the directions of incident as well as the scattered electric field vectors, respectively. As $|R_{ij}|=|R_{ji}|$ (i, j denote the axes) for all the allowed modes of SnO, we studied the parallel $[Z(XX)\bar{Z}]$ and perpendicular $[Z(XY)\bar{Z}]$ polarization conditions only.

Raman spectra of the textured SnO(001) crystals at two different polarization conditions and for two different orientations are shown in figure 3.

Two Raman modes are observed at 114 and 211 cm^{-1} in the $Z(XX)\bar{Z}$ configuration [12–14] as expected from our previous discussion. Whereas in the case of $Z(XY)\bar{Z}$ polarization condition, intensity of both the peaks falls down rapidly (figure 3a). The depolarization ratios ρ ($=I_{\perp}/I_{\parallel}$, where $I_{\perp}$ and $I_{\parallel}$ being the intensities of the Raman modes in the perpendicular $[Z(XY)\bar{Z}]$ and parallel $[Z(XX)\bar{Z}]$ configurations, respectively) of these two modes are ρ (114 cm^{-1}) = 0.16 and ρ (211 cm^{-1}) = 0.03. The small values of ρ make the modes highly polarized considering the Placzek's polarizability approximation value of 0.75. It is also clear that the above two observed modes are A_{1g} and B_{1g}, as those are the only allowed modes in the $Z(XX)\bar{Z}$ configuration. However, assignment of the individual mode either for A_{1g} or B_{1g} is not possible from the above study.

For assigning the modes individually, we rotated the crystal by an angle of 45° around Z-axis (c-axis of the crystal) and repeated the polarized Raman experiment. Figure 4 shows the schematic of the generation of scattered modes for two different crystal orientations of SnO(001) single crystal. In the first case (top panel of figure 4), the electric field vector of the incident wave ($\boldsymbol{E}_{\rm i}$) is parallel to the X-axis i.e., a-axis of the crystal frame. So, the x and y components of the incident electric field are $\boldsymbol{E}_{x\rm i} = \boldsymbol{E}_{\rm i}$ and $\boldsymbol{E}_{y\rm i} = 0$, respectively.

Using equation (1), one can predict the direction of scattered electric field vector for both A_{1g} and B_{1g} modes. For A_{1g} mode, the scattered electric field vectors are $\boldsymbol{E}_{sx} = a\boldsymbol{E}_{\rm i}$ and $\boldsymbol{E}_{sy} = 0$. Similarly, for B_{1g} mode, two components are $\boldsymbol{E}_{sx} = c\boldsymbol{E}_{\rm i}$ and $\boldsymbol{E}_{sy} = 0$. So, the scattered electric field ($E_{\rm s}$) for both the A_{1g} and B_{1g} modes are along X-axis i.e., parallel to $\boldsymbol{E}_{\rm i}$ and therefore, both the modes are allowed for $Z(XX)\bar{Z}$ configuration only. In the second case (bottom panel of figure 4), the crystal is rotated by an angle 45° around the Z-axis. So, $\boldsymbol{E}_{\rm i}$ has both x and y components $\boldsymbol{E}_{x\rm i}$ and $\boldsymbol{E}_{y\rm i}$ in the crystal frame. Hence, $\boldsymbol{E}_{\rm s}$ for A_{1g} mode also has two components $\boldsymbol{E}_{\rm sx} = a\boldsymbol{E}_{x\rm i}$ and $\boldsymbol{E}_{\rm sy} = a\boldsymbol{E}_{y\rm i}$. The resultant $\boldsymbol{E}_{\rm s}$ is along $\boldsymbol{E}_{\rm i}$, as for A_{1g} mode, both xx and yy Raman tensor components are equal in magnitude and sign. On the other hand, xx and yy tensor components are equal with opposite sign for B_{1g} mode. Thus, scattered electric field for B_{1g} mode has components, $\boldsymbol{E}_{\rm sx} = c\boldsymbol{E}_{x\rm i}$ and $\boldsymbol{E}_{\rm sy} = -c\boldsymbol{E}_{y\rm i}$. The total $\boldsymbol{E}_{\rm s}$ is the vector sum of $\boldsymbol{E}_{\rm sx}$ and $\boldsymbol{E}_{\rm sy}$ and is along perpendicular direction of $\boldsymbol{E}_{\rm i}$. So, A_{1g} mode is allowed only in the parallel $[Z(XX)\bar{Z}]$ polarization configuration, and B_{1g} mode is allowed only in the perpendicular $[Z(XY)\bar{Z}]$ polarization configuration.

The Raman spectra of the 45° oriented crystal for different polarization conditions are shown in figure 3b. In the $Z(XX)\bar{Z}$ configuration, a sharp Raman peak is observed at 211 cm^{-1}. Whereas in the case of $Z(XY)\bar{Z}$ polarization condition, a sharp peak is observed at 114 cm^{-1}. According to the above discussion, we can assign the Raman modes observed at 211 cm^{-1} as A_{1g} and 114 cm^{-1} as B_{1g} uniquely, as A_{1g} and B_{1g} modes are allowed only in the parallel $[Z(XX)\bar{Z}]$ and in the perpendicular $[Z(XY)\bar{Z}]$ polarization configurations, respectively. Both A_{1g} mode in $Z(XY)\bar{Z}$ and B_{1g} mode in $Z(XX)\bar{Z}$ conditions are present with negligible intensities, possibly because of polarization leaking considering lack of perfect levelling of the crystal orientations. The ρ (I_{XX}/I_{XY}; 114 cm^{-1}) = 0.23 and ρ (I_{XY}/I_{XX}; 211 cm^{-1}) = 0.11 are also calculated to be negligible to show strong polarization of the modes. Thus, the phonon assignment is performed relatively easily with minimal data collection for a diatomic molecule with tetragonal symmetry having a number of symmetry elements.

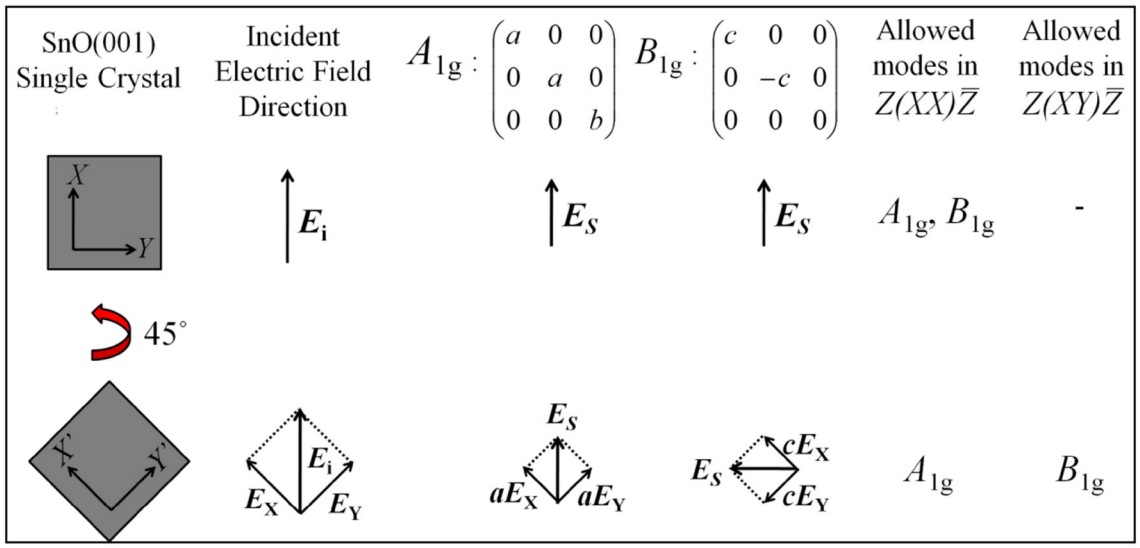

Figure 4. Direction of electric field vector with respect to incident electric field vector and prediction of allowed Raman modes in parallel and perpendicular polarization conditions for two different crystal orientations of the SnO(001) single crystal.

4. Conclusions

In conclusion, cubic- and cuboidal-shaped single crystals of SnO(001) were synthesized by the one-step hydrothermal method. Crystalline phase and orientation are identified using high resolution electron microscopy assisted structural and Raman spectroscopic studies. At the same time, polarized Raman studies of the sample only in two different crystal orientations: (i) X-axis parallel to incident electric field vector and (ii) oriented at an angle of 45° around the Z-axis to incident electric field vector, confirming the crystal orientation. It also helps in solving the conflict in the assignment of the individual Raman modes uniquely, where 114 cm^{-1} mode is identified as B_{1g}.

Acknowledgement

We thank V Sridharan of CMPD for his advice in preparing the sample and for his critical reading of the manuscript.

References

[1] Ogo Y, Hiramatsu H, Nomura K, Yanagi H, Kamiya T, Hirano M *et al* 2008 *Appl. Phys. Lett.* **93** 32113
[2] Liang L Y, Liu Z M, Cao H T and Pan X Q 2010 *ACS Appl. Mater. Interfaces* **2** 1060
[3] Zhao Q and Bartsch R A 1995 *J. Appl. Polym. Sci.* **57** 1465
[4] Han Z, Guo N, Li F, Zhang W, Zhao H and Qian Y 2001 *Mater. Lett.* **48** 99
[5] Pan X Q and Fu L 2001 *J. Appl. Phys.* **89** 6048
[6] Uchiyama H and Imai H 2007 *Cryst. Growth Des.* **7** 841
[7] Ning J, Jiang T, Men K, Dai Q, Li D, Wei Y *et al* 2009 *J. Phys. Chem. C* **113** 14140
[8] Kumar B, Lee D H, Kim S H, Yang B, Meang S and Kim S W 2010 *J. Phys. Chem. C* **114** 11050
[9] Aurbach D, Nimberger A, Markovsky B, Levi E, Sominski E and Gedanken A 2002 *Chem. Mater.* **14** 4155
[10] Dai Z R, Pan Z W and Wang Z L 2003 *Adv. Funct. Mater.* **13** 9
[11] Orlandi M O and Leite E R 2006 *J. Phys. Chem. B* **110** 6621
[12] Geurts J, Rau S, Richter W and Schmitte F J 1984 *Thin Solid Films* **121** 217
[13] Wang X, Zhang F X, Loa I, Syassen K, Hanfland M and Mathis Y L 2004 *Phys. Status Solidi B* **241** 3168
[14] Luo H, Liang L Y, Cao H T, Liu Z M and Zhuge F 2012 *ACS Appl. Mater. Interfaces* **4** 5673
[15] Liu Q, Liang L, Cao H, Luo H, Zhang H, Li J *et al* 2015 *J. Mater. Chem. C* **3** 1077
[16] Iqbal M Z, Wang F, Din R U, Rafique M Y, Javed Q U A, Ullah A *et al* 2012 *Mater. Lett.* **78** 50
[17] Hota M K, Caraveo-Frescas J A, McLachlan M A and Alshareef H N 2014 *Appl. Phys. Lett.* **104** 152104
[18] Peltzer y Blanca E L, Svane A, Christensen N E, Rodriguez C O, Cappannini O M and Moreno M S 1993 *Phys. Rev. B: Condens. Matter Mater. Phys.* **48** 15712
[19] Koval S, Burriel R, Stachiotti M G, Castro M, Migoni R L, Moreno M S *et al* 1999 *Phys. Rev. B: Condens. Matter Mater. Phys.* **60** 14496
[20] Sornadurai D, Sridharan V, Ajikumar P K, Ravindran T R and Subramanian N 2017 *AIP Conf. Proc.* **1832** 140049
[21] Dai Z R, Pan Z W and Wang Z L 2002 *J. Am. Chem. Soc.* **124** 8673
[22] Doh W H, Jeong W, Lee H, Park J and Park J Y 2016 *Nanotechnology* **27** 335603
[23] Kroumova E, Aroyo M I, Perez Mato J M, Kirov A, Capillas C, Ivantchev S *et al* 2003 *Phase Transit.* **76** 155